


Summer 2024

Understanding the Impact of Process Interruption on Mechanical Properties in Metal Additive Manufacturing: A Comprehensive Investigation

Poojith C. Chigurupati

Follow this and additional works at: <https://digitalcommons.georgiasouthern.edu/etd>

 Part of the [Manufacturing Commons](#), and the [Other Mechanical Engineering Commons](#)

Recommended Citation

Chigurupati, Poojith C., "Understanding the Impact of Process Interruption on Mechanical Properties in Metal Additive Manufacturing: A Comprehensive Investigation" (2024).

Electronic Theses and Dissertations. 2829.

<https://digitalcommons.georgiasouthern.edu/etd/2829>

This thesis (open access) is brought to you for free and open access by the Jack N. Averitt College of Graduate Studies at Georgia Southern Commons. It has been accepted for inclusion in Electronic Theses and Dissertations by an authorized administrator of Georgia Southern Commons. For more information, please contact digitalcommons@georgiasouthern.edu.

UNDERSTANDING THE IMPACT OF PROCESS INTERRUPTION ON MECHANICAL PROPERTIES IN
METAL ADDITIVE MANUFACTURING: A COMPREHENSIVE INVESTIGATION

by

POOJITH CHOWDARY CHIGURUPATI

(Under the Direction of Hossein Taheri)

ABSTRACT

Metal additive manufacturing techniques enable rapid prototyping and on-demand manufacturing while improving supply chain resiliency. Changes in microstructure and micro-mechanical characteristics of 3D printed metal parts occur due to the influence of process interruptions on melting-solidification cycles during the layer evolution in additive manufacturing processes. The process interruption can deteriorate the structural integrity of the 3D printed parts and generate micro-flaws in the interruption region. Manufacturing post-processing techniques such as Heat-Treatment methods can enhance the mechanical properties of the parts. Since variations commonly happen at the layer level, the investigation of mechanical properties must be done such that these variations can be effectively identified, evaluated, and used to inform post-processing needs. Hence, this study investigates the influence of process interruption on the micro-mechanical properties of the metal 3D printed parts for stainless steel parts with and without post-processing. Accordingly, various stainless steel 316L parts are fabricated using powder-bed fusion additive manufacturing process. Manufacturing processes included different process lags. Nano-indentation testing is used to measure the elasticity and hardness. Measurements are recorded in a matrix grid form covering the interruption region of the manufacturing process. Measurement results of measurement are analyzed to detect potential

variations caused by the process interruption. To investigate the influence of the post-processing procedures on the enhancements of mechanical properties of the parts, a group of parts were heat-treated in a vacuum furnace. Micro-mechanical properties were also measured for the parts with heat-treated post-processing. Results indicate that process interruptions and lags alter the mechanical properties of the parts; however, the variation can be reduced using post-processing procedures.

INDEX WORDS: Additive Manufacturing (AM); Indentation Test; Material Properties; Process Interruption

UNDERSTANDING THE IMPACT OF PROCESS INTERRUPTION ON MECHANICAL PROPERTIES IN
METAL ADDITIVE MANUFACTURING: A COMPREHENSIVE INVESTIGATION

by

POOJITH CHOWDARY CHIGURUPATI

B. Tech. Mechanical Engineering, Velagapudi Ramakrishna Siddhartha Engineering College,
India, 2021

M.S. Applied Engineering: Advanced Manufacturing Engineering, United States, Georgia
Southern University, 2024

A Thesis Submitted to the Graduate Faculty of Georgia Southern University

in Partial Fulfillment of the Requirements for the Degree

MASTER OF APPLIED ENGINEERING

ALLEN E. PAULSON COLLEGE OF ENGINEERING

© 2024

POOJITH CHOWDARY CHIGURUPATI

All Rights Reserved

UNDERSTANDING THE IMPACT OF PROCESS INTERRUPTION ON MECHANICAL PROPERTIES IN
METAL ADDITIVE MANUFACTURING: A COMPREHENSIVE INVESTIGATION

By

POOJITH CHOWDARY CHIGURUPATI

Major Professor:

Hossein Taheri

Committee:

Dean Snelling

Jingjing Qing

Electronic Version Approved:

July 2024

DEDICATION

Dedicated to my parents and my brother who has been my inspiration to improve myself and to the person I'm now. To my friends and family who have been there since day one.

ACKNOWLEDGMENTS

I would like to thank:

- Dr. Hossein Taheri for helping me and believed in me will all the projects so far and upcoming projects.
- Dr. Snelling for introducing me to Additive Manufacturing techniques
- Andrew Michaud for always teaching me new machinery and fixing them back if I break them.
- Dr. Silwal and his research team
- Department of Manufacturing Engineering.

TABLE OF CONTENTS

	Page
ACKNOWLEDGMENTS	3
TABLE OF CONTENTS.....	4
LIST OF TABLES	6
LIST OF FIGURES	7
CHAPTER 1: INTRODUCTION.....	9
CHAPTER 2: LITERATURE REVIEW	10
2.1 Causes and effects of Process Interruption in metal AM.....	15
2.1.1 Causes and effects of Process Interruption in PBF	15
2.1.2 Causes and effects of Process Interruption in WAAM.....	16
CHAPTER 3: METHODS	18
3.1 Printing Process	18
3.1.1 L-PBF Samples	18
3.1.2 WAAM Samples	21
3.2 Heat Treatment.....	24
3.3 Sample Preparation	26
3.4 Nano Indentation.....	27
CHAPTER 4: DISCUSSION/RESULTS	32

4.1	Indentation test.....	32
4.1.1	L-PBF (Laser Powder Bed Fusion).....	32
4.1.2	WAAM Samples	35
4.2	Statistical Analysis using ANOVA Test.....	36
4.2.1	ANOVA analysis of L-PBF samples	37
4.2.2	ANOVA Analysis of WAAM Samples	44
4.3	Microscopic Images	46
4.4	Future Work	49
CHAPTER 5: CONCLUSION		51
REFERENCES		53

LIST OF TABLES

	Page
Table 1: Process Parameters used for sample fabrication.....	20
Table 2: Build report for each print	20
Table 3: Mechanical Properties and Wire Composition	23
Table 4: Nano Indentation Parameters.....	29
Table 5: Hardness of As-Built of L-PBF samples	37
Table 6 : Hardness of HT Samples of L-PBF samples	39
Table 7: Elasticity of As-Built of L-PBF samples	41
Table 8: Elasticity of HT Samples of L-PBF samples.....	43
Table 9: Hardness of As-built VS HT of WAAM sample.....	45
Table 10 : Elasticity of As-built VS HT of WAAM sample.....	46

LIST OF FIGURES

	Page
Figure 1. Relationship linking various potential AM process interruption causes	12
Figure 2. Methodology used for this Study	17
Figure 3. L-PBF system used for sample fabrication	18
Figure 4. CAD model of Parameter B and BH	19
Figure 5. Sample Placement on Build plate(left) and Build Orientation (right).....	21
Figure 6. WAAM system used for fabrication of samples	22
Figure 7. As-Built WAAM Sample	23
Figure 8. Solar Vacuum Furnace	25
Figure 9. Heat Treatment Process	25
Figure 10. Samples sectioned for mounting. WAAM samples (left) & LPBF (right).....	26
Figure 11. a) print -1 parameter D as it has 4 lines b) print-2 parameter B as it has 2 lines and interruption line in middle c) Print -3 parameter E as it has one line on the farther side of interruption region	27
Figure 12. Measurement of load and penetration depth and related load-penetration curve.....	29
Figure 13. Matrix of the Indentation on the L-PBF samples	30
Figure 14. Indentation Matrix used for WAAM Samples	30
Figure 15. Sample Under the Nano Indenter- (a) Under the indenter head and (b) Under 20x microscope head.....	31
Figure 16. Mapping of Hardness values of as-built samples	32

Figure 17. Mapping of Hardness values of Heat-treated samples	33
Figure 18. Mean & SD hardness comparison between As-built & Heat-treated L-PBF samples	34
Figure 19. Mean & SD Elasticity comparison between As-built & Heat treated samples	35
Figure 20. Comparison of Hardness values of all indentation on WAAM sample	36
Figure 21. Comparison of Elasticity values of all indentation on WAAM sample	36
Figure 22. Indentation points with a porosity line on Print-3 for parameter E with 5x magnification (As-Built)	47
Figure 23. Indentation points without porosity line on Print-3 for parameter E with 5x magnification (Heat Treated)	47
Figure 24. Print-2 of Parameter B under 20x magnification	48
Figure 25. Print-3 of Parameter B under 20x magnification	49

CHAPTER 1

INTRODUCTION

Purpose of the Study

Additive manufacturing/3D printing (AM/3DP) creates a part by adding material layer by layer using a CAD file, which is unlike traditional manufacturing processes which consist of subtracting materials. AM/3DP has advantages over the traditional manufacturing including flexibility, better customization, and design freedom. There are various AM/3DP techniques including Binder Jetting, Selective Laser Sintering (SLS), Selective Laser Melting (SLM), and Direct Energy Deposition (DED). Due to numerous influences on printing processing, defects are common in parts and can affect the mechanical properties [1-4], in addition process interruption can happen over the printing process due to various situations such as power run off or fault in control software of the machine. There have been studies investigating the process parameters and the type of defects like lack of fusion (LOF), ball peening, keyhole pores have on the part [5-9]. However, there are limited studies on the impact process interruption has on the mechanical properties. Research motivation stands behind this to understand the effects of process interruption on mechanical properties of additively manufactured metal parts and to investigate how it affects the hardness and elasticity of the part.

CHAPTER 2

LITERATURE REVIEW

Like any other manufacturing process, AM/3DP technologies can be subject to machine failures, power outages, and other interruptions during printing process. It is important to investigate how these interruptions can have effects on the part's mechanical properties. These interruptions can occur because of machine failure due to excessive levels of oxygen in the chamber or unexpected power outages. This leads to changes in the thermal history, exposure to oxygen in the part, and other defects which could negatively affect the mechanical properties of the part. However, the findings from these reports are fragmented and lack a structured approach toward reaching robust conclusions. This deficiency arises from a dearth of scientific investigations specifically addressing this aspect. Mahtabi et al studied the effect that interruption time would have on dissimilar materials and by changing the exposure time, heat treating the samples, and surface finishing the others they found that there were no distinctive changes in tensile strength and microhardness test in materials used. The locations at which they failed were not consistent as well, but longer exposure meant more likely to fail at an interruption location [10]. In his experiment Stokes found that at 24 hours exposure time, half of the parts fractured at the interrupted location. Stokes contributed this to potentially the introduction of oxides and age hardening in the sample [11]. Terrazas-Najera et al. study got similar findings using aluminum alloy Al-Si-10Mg in that there was no variance in tensile and hardness performance as well as no change in the microstructure [12]. This is contradictory to Hammond et al.'s study of Al-Si-10Mg alloy. In Hammond's study a 10 percent difference in tensile strength between non-interrupted and interrupted samples were found [13].

As previously mentioned, the studies of process interruption are contradictory for PBF process and focus on tensile testing, hardness, and microstructure analysis, but there is no or little on its effect on fatigue properties. Taheri et al. used NDT-RAM and was able to detect the difference between the interrupted and uninterrupted location in wire arc additive manufactured (WAAM) part [14].

For industries, such as aerospace and automotive, to adopt metal AM/3DP technologies at larger volumes, the impact of AM/3DP process interruption on the part's properties must be understood. Based on the aforementioned literatures, the following can be concluded. AM/3DP printing mechanisms and process parameters greatly influence the material properties and reliability of parts produced using AM/3DP. When disrupted, interlayer time, temperature gradients, thermal cycles, the melt pool, etc. all can lead to material property defects that jeopardize the mechanical properties of AM/3DP parts. This relationship stemming from AM/3DP process interruption to the mechanical properties is summarized in Figure 1.

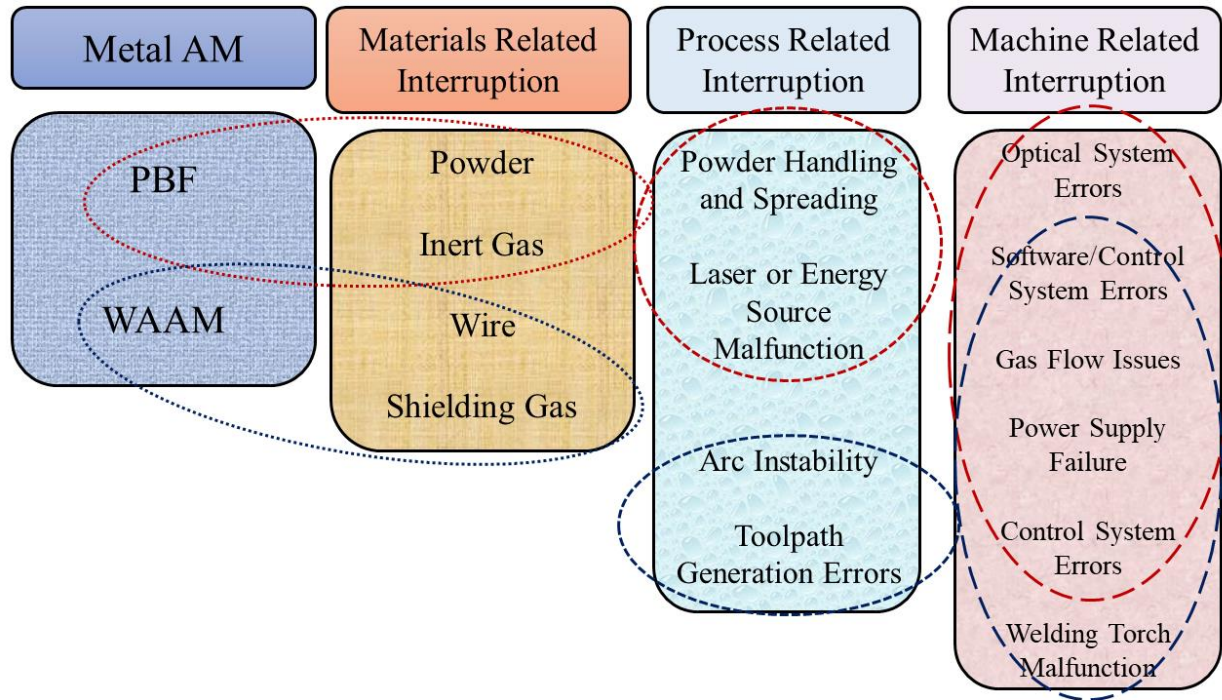


Figure 1. Relationship linking various potential AM process interruption causes

Figure 1 presents a categorized overview of interruptions that can occur in Metal Additive Manufacturing (AM), focusing on two specific processes: Powder Bed Fusion (PBF) and Wire Arc Additive Manufacturing (WAAM). The interruptions are divided into three main categories: Materials Related Interruption, Process Related Interruption, and Machine Related Interruption. The connections between each type of interruption and the specific AM processes (PBF and WAAM) are indicated by dashed lines.

The primary difference between metal AM/3DP and polymer/plastic 3D printing lies in the melting and solidification process of the raw materials, whether in powder or wire form. Metal AM/3DP operates at elevated temperatures and requires a higher energy density [15].

The attributes inherent in additive manufacturing, such as tool-less production, rapid turnaround times coupled with precision, design freedom, intricate part fabrication, weight reduction, component integration, and functional design optimization, are drawing significant attention within the metal additive manufacturing sector. This heightened interest spans across various industries, including aerospace, oil and gas, marine, and automotive applications [16].

In this study, two major and widely used metal AM/3DP techniques: Laser Powder Bed Fusion (L-PBF) and Wire Arc Additive Manufacturing (WAAM). These methods are chosen because they are significant within the field of metal AM/3DP and offer distinct advantages and characteristics for comparison. By focusing on these two techniques, the article aims to provide a more in-depth analysis rather than attempting to cover a broader range of methods.

Powder Bed Fusion (PBF) is a commonly used technique in metal AM/3DP. It creates parts by spreading thin layers of powder over a build plate, which are then melted or sintered and fused together using a heat source, such as a high-power laser or an electron beam. The build plate moves down, and this process is repeated until the part is fully manufactured. Several parameters directly influence the part's outcome and quality, including laser power, hatch size, scan speed, build orientation, part orientation, and scan orientation [17]. The scanning speed significantly influenced the melting pool boundaries, residual pores, solidification cells, nano-inclusions, as well as grain size and distribution. The ultimate tensile strength (UTS) slightly decreased with increasing energy density, while the elongation to failure exhibited the opposite trend [18]. Numerous studies have demonstrated that deviations from the optimal and recommended processing parameters in PBF can lead to flaws in the manufactured parts. The

two primary types of these flaws are gas porosity and lack of fusion, both of which can degrade the mechanical performance of the parts. The mechanisms behind the generation of these flaws, as well as their impact on the static and dynamic material properties and mechanical performance of the parts, are not yet fully understood or quantified [12]. The fabrication of 316L stainless steel using selective laser melting (SLM) to produce specimens with high strength and ductility has been documented in the literature[19] [20]. It was observed that the manufacturing orientation significantly influenced the mechanical properties: specimens built in the horizontal direction typically exhibited higher yield strength and tensile strength compared to those built in the vertical (built-up) direction. Zhang et al. discovered that optimizing the placement orientation and scanning angle resulted in highly densified 316L stainless steel, achieving a maximum tensile strength of 657 MPa[18][21], [22]

In the field of AM/3DP, Wire Arc Additive Manufacturing (WAAM) is attracting significant interest for producing large components with moderate geometric complexity [23]. Two key characteristics of WAAM that result in significant cost and time savings compared to PBF methods are the use of wire as the feedstock and the employment of an electric arc as the fusion source for building components layer by layer. [23], [24]. Consequently, various material and process-related parameters can influence the performance of the WAAM process, including the thermal and chemical properties of the wire materials and the characteristics of the electric arc. In WAAM, the paths of thermal dissipation and the significant temperature differences between the substrate and the in-situ layer can lead to heat accumulation. This heat buildup can cause variations in arc shape and metal transfer behavior, leading to changes in material characteristics and, in extreme cases, interrupting the manufacturing process. [25].

2.1 Causes and effects of Process Interruption in metal AM

Due to process specific factors and parameters involved in each metal AM/3DP techniques, the causes and consequent effects of the process interruptions could be different and must be investigated separately for each AM/3DP techniques.

2.1.1 Causes and effects of Process Interruption in PBF

Process interruptions in PBF additive manufacturing can result from various factors such as powder delivery issues, powder spreading problems, and heat source malfunction. Studying interruptions in PBF additive manufacturing is essential for optimizing processes, ensuring quality, reducing costs, enhancing reliability, promoting safety and environmental sustainability, driving technological innovation, and maintaining competitiveness in the industry. This section outlines the primary causes of process interruption in PBF additive manufacturing and discusses their potential impact on the properties of materials fabricated through PBF.

J. Richter et al. used EBSD to investigate process interruption on AlSi12 manufactured by PBF-LB/M which showed the process-induced thermal history primarily drives this phenomenon. At the area of process interruption, a distinct distortion in the microstructure is directly visible on the surface. This local microstructure mismatch is attributed to residual stresses and non-uniform thermal expansion [26].

For AlSi10Mg, the observations revealed that the Al-Si eutectic phases exhibited similar features, including comparable sizes and morphology of the α -Al cells. As discussed in this and other studies, there was a tendency for α -Al cells to refine below and above the melt-pool band, whereas coarser cells were evident within the melt-pool bands. These findings align with data indicating the static tensile properties remain unchanged. Similarly, for Inconel alloys,

neither the microstructure nor mechanical properties appear to be affected by the interruption, with the obtained values remaining within the range of expected experimental variations [27].

2.1.2 Causes and effects of Process Interruption in WAAM

Various factors may lead to interruptions in the WAAM process and can impact the final properties of manufactured parts. It is crucial to identify and address these potential causes of interruptions to optimize the performance, reliability, and productivity of WAAM processes [14]. This section presents the most crucial causes of process interruption in WAAM and their potential influence on WAAM manufactured materials properties.

WAAM may be paused if the feeding spool runs out of wire or if there is a wire break. Although these interruptions are rare and can be quickly resolved by replacing the spool, it is crucial to estimate the required amount of feeding material before starting the manufacturing process. Accurate estimation involves knowing the weight and volume of the part to be manufactured, the estimated rate of wire usage during the WAAM deposition, and consulting expert knowledge. This approach significantly improves estimation accuracy and reduces the likelihood of interruptions due to wire depletion. When multiple wire spools are needed to complete a part, pre-preparing the required number of spools can minimize downtime. For instance, manufacturing a part measuring 25.4x127x76.2mm (approximately 11.5x5x3 inches) in stainless steel would require at least 5.5 kg (about 12.13 pounds) of wire.

Numerous researchers have demonstrated that the composition and physical properties of the raw material are fundamental factors that contribute significantly to the final properties, quality, and integrity of AM/3DP manufactured parts [28]. It is crucial to consider this point when replacing wire spools, ensuring that a new spool with identical raw material properties (ideally from the same manufacturer and brand) is used when necessary. Microhardness tests indicated higher

values for the block coupon. Porosity analysis revealed lack-of-fusion defects, primarily in the first deposition layers. The thin-walled coupon's shorter inter-layer time reduced the cooling rate, resulting in coarser grain size and lower UTS. Grain size increased from bottom to top of each layer due to cooling rate variations[29].

For this Study, All the samples were fabricated in-house, and the methodology used for the sample fabrication and testing is shown in *Figure 2*

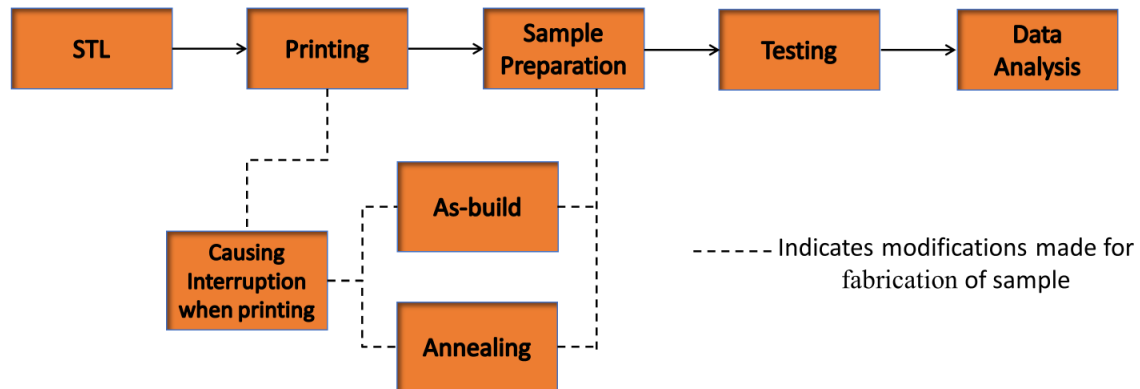


Figure 2. Methodology used for this Study

CHAPTER 3

METHODS

The Methods are divided into various sections, each section gives a detailed description of how the samples are designed, manufactured, heat treated, prepared and testing to obtain the results which can give us a better understanding of the impact of the process interruption of AM samples.

3.1 Printing Process

In this section, it is explained how the samples are designed and how they are manufactured using the L-PBF & WAAM techniques.

3.1.1 L-PBF Samples

Laser Powder Bed Fusion (L-PBF) method has been used to produce the AM parts. The test samples are made of stainless steel 316L (SS-316L), The as-built original dimensions of the structure are 45 mm x 12 mm x 10 mm with a support's height of 5mm. The build was completed using gas atomized powder with $45 \pm 15 \mu\text{m}$ particle size with the process parameters presented in **Error! Reference source not found..** The time for each print was reported in *Table 2*. All the samples were printed using Farsoon FS-271 M which is shown in *Figure 3*.



Figure 3. L-PBF system used for sample fabrication

Once the CAD design is completed the file is exported as STL file compiles with the printing software used in the Farsoon machine. Figure 4 shows the CAD model of parameter B, where BH indicate that the sample needs to be Heat treated.

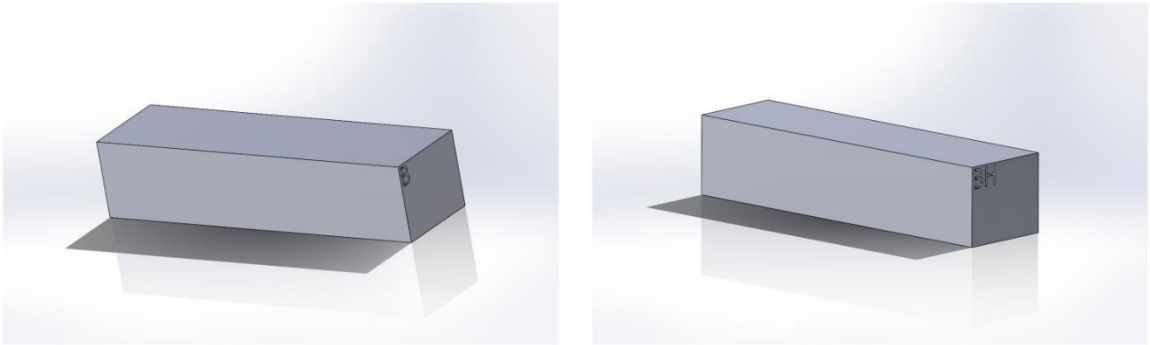


Figure 4. CAD model of Parameter B and BH

Table 1: Process Parameters used for sample fabrication.

Part Name	Laser Power	Scan Speed
A (optimum parameters)	225w	1000mm/s
B (decreased Laser power with optimum scan speed)	200w	1000mm/s
C (Increased Laser power with optimum scan speed)	250w	1000mm/s
D (Optimum Laser power with decreased scan speed)	225w	800mm/s
E (Optimum Laser power with increased scan speed)	225w	1200mm/s

Table 2: Build report for each print

Print	Build Time	Interruption Time
1	29 hours	30 mins
2	31 hours	2 hours
3	41 hours	12 hours

Figure 5 shows the Build Orientation and Placement of each parameter samples for each print. For all the prints the interruption region was maintained constant, and the prints were paused exactly at 25mm from the bottom for each parameter and the interruption region is at 20mm without support. Once the prints are completed then samples are sectioned using bandsaw and cleaned off.

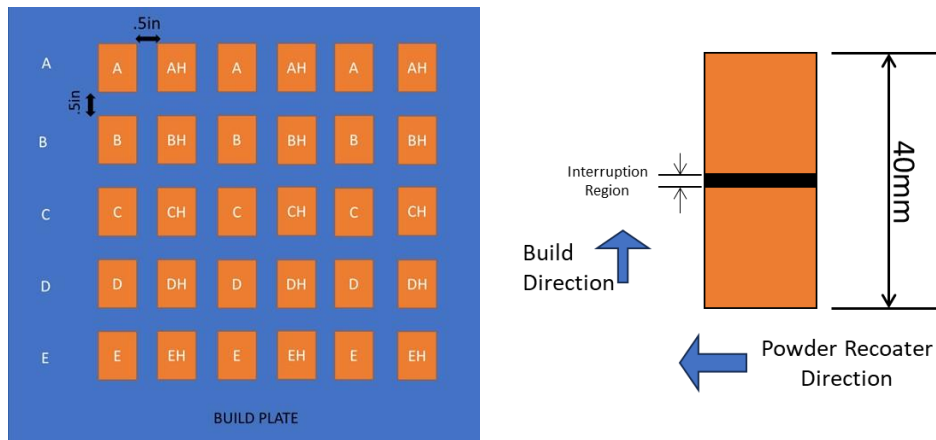


Figure 5. Sample Placement on Build plate(left) and Build Orientation (right)

3.1.2 WAAM Samples

The mechanical properties and wire composition used in this study have been presented in Table 3 . In this experiment, 75% Argon and 25% CO₂ compressed gas were employed during the welding process, so that the mechanical properties of the welded part are estimated as shown in Table 3, representing that the Yield strength and tensile strength of sample 1 (LA-90) are 620 MPa and 705 MPa respectfully, and percentage of

elongation is 26. For the Fabrication of WAAM samples KUKA robotic arm (Model KR 6 R900 six) with transport positioning of 6-axis movements within the 900mm range was used shown in Figure 6. The control display is connected to the robotic arm for operation and control of the process. A low carbon steel (1.1 mm diameter) GMAW (Gas Metal Arc Welding) wire feedstock was used for manufacturing sample 1. A high-performance welding device (K3451-1) was connected to the robotic arm as a power source, which can provide faster travel speeds, lower spatter generation, superior gap bridging, and excellent penetration. Figure 7 shows the WAAM sample being fabrication.



Figure 6. WAAM system used for fabrication of samples

Table 3: Mechanical Properties and Wire Composition

(LA-90, 1.1 mm)			
Mechanical Properties			
AWS A5.28/A5.28M and with 75% of Ar, 25% of CO ₂	Yield Strength Mpa (ksi)	Tensile Strength MPa (ksi)	Elongation %
	620(90)	705 (102)	26
Wire Composition			
AWS A5.28/A5.28M and typical results	%C 0.09-0.11	%Mn 1.63-1.74	%Si 0.56-0.64
	%Mo 0.43-0.46	%S ≤0.010	%P 0.007 -0.016
	%Ni ≤0.04	%Cu(total) 0.16-0.22	



Figure 7. As-Built WAAM Sample

3.2 Heat Treatment

The samples were put in a basket made of steel; all the samples were heat treated (HT) using a vacuum furnace with nitrogen gas used for forced cooling cycle. It is known that post-heat treatments after the SLM process induces microstructural evolution and alternation of mechanical and functional properties

It is established that post-heat treatments following the Selective Laser Melting (SLM) process lead to microstructural changes and alterations in mechanical and functional properties [30], [31]. However, the impact of heat treatment on SLM SS316's material properties remains incompletely understood, as noted in several studies. Kamariah et al. [32] observed a decline in microhardness of SLM SS316L with higher heat treatment temperatures, attributed to reduced δ -ferrite volume. Salman et al. investigated the microstructure and mechanical properties of SLM SS316L pre- and post-heat treatment, noting an increase in cell size and a decrease in mechanical strength with rising heat treatment temperatures.[33]

The samples were notched prior to the HT process to differentiate between prints, the thermocouple used has a work gauge, at a ramp up rate of $2^{\circ}\text{C}/\text{min}$. Once the furnace temperature reached 885°C the samples were soaked for 4hrs and 30 mins, next the temperature was dropped to 10°C with force vacuum cooling at +5psi. Once the temperature reaches 10°C the samples were re-heated to a temperature of 677°C with a ramp up rate of 1°C and then the samples were soaked for 50 minutes, and furnace cooled until it reached room temperature. The entire HT process took around 30 hrs. *Figure 9*, shows the heat treatment process used for this study. The equipment used for this study is Solar Manufacturing SF-204 show in *Figure 8*.

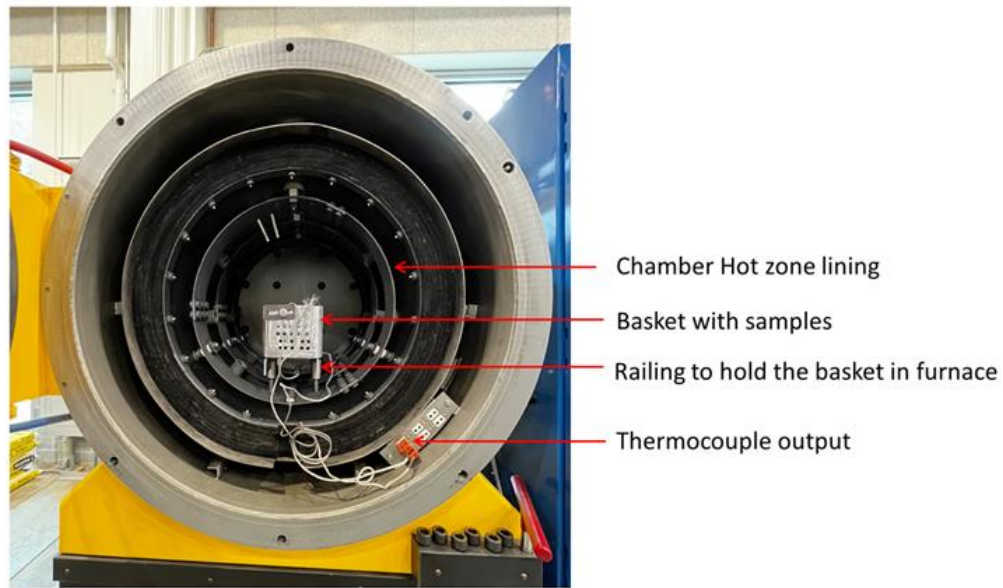


Figure 8. Solar Vacuum Furnace

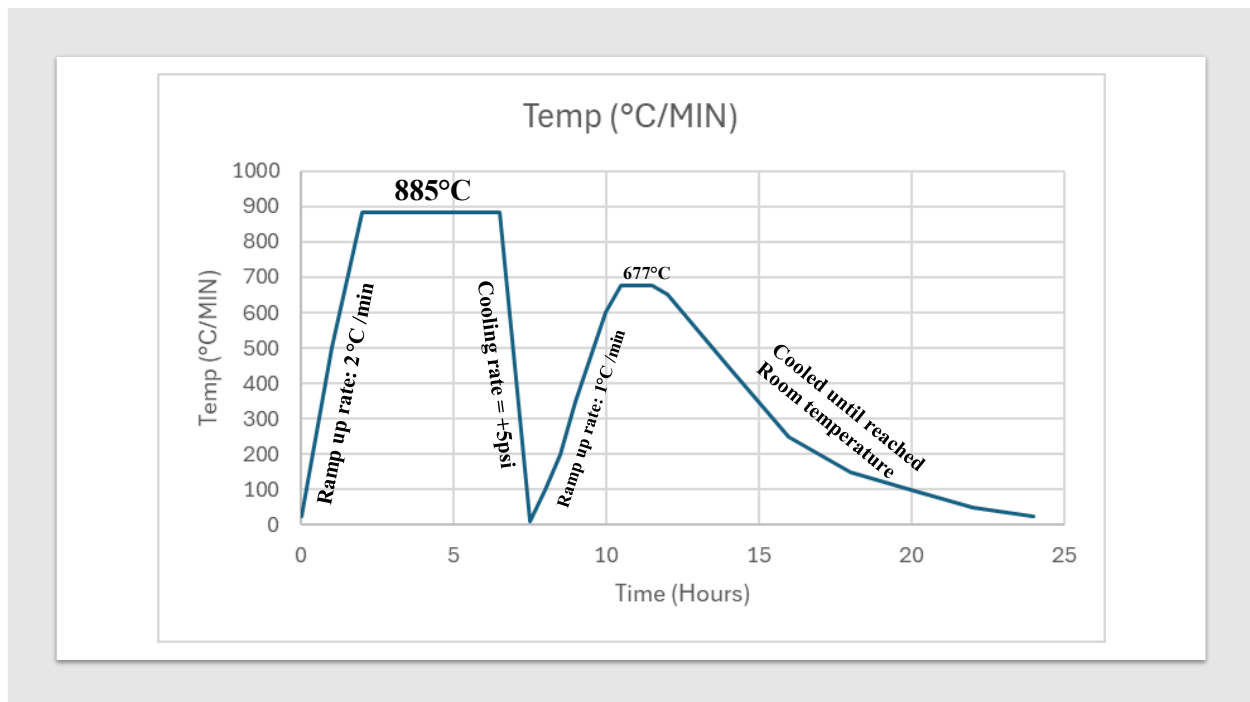


Figure 9. Heat Treatment Process

3.3 Sample Preparation

Once the samples were separated from the build plate smaller sections (12 mm by 10 mm cross-section) in interruption region were extracted from the original as-built structure as shown in Figure 10. Notches were made on these sections right on the interruption location for easy identification of the samples as shown in Figure 11. Then the samples were mounted using 1.25in phenolic powder using pace technology TP-7100s and polished using an auto polisher from pace technologies 400, 600, 800 & 1200 grinding papers along with polishing agents 9 μ m & 3 μ m diamond Suspension polycrystalline, were considered for the indentation tests. Samples were polished until a mirror like finish is obtained.



Figure 10. Samples sectioned for mounting. WAAM samples (left) & LPBF (right)

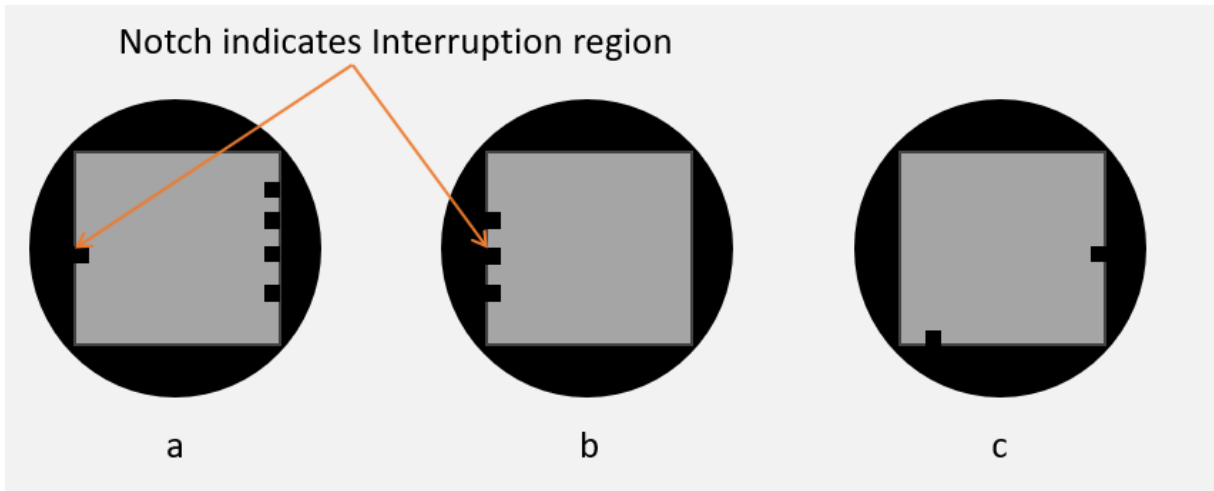


Figure 11. a) print -1 parameter D as it has 4 lines b) print-2 parameter B as it has 2 lines and interruption line in middle c) Print -3 parameter E as it has one line on the farther side of interruption region

3.4 Nano Indentation

To quantify the effect of the process interruption on mechanical properties of parts fabricated using LPBF AM, the indentation material testing technique is used for testing and evaluation of the parts. The indentation testing technique provides data on two important material properties: modulus of elasticity and hardness. The main reason for using nanoindentation is that nanoindentation technique is very precise and efficient in measuring these two important material properties for a sample in just one indentation test (load vs displacement curve) [34]. The indentation method is a widely recognized technique for determining the elastic modulus and hardness of materials based on the Oliver and Pharr theory[35]. Moreover, the test is done on a very small scale which opens the opportunity to evaluate the localized material properties or changes in desired locations and/or mapping with spatial distances as low as 10-50 μm . As

mentioned previously, before testing the samples, precise sample preparation is necessary to ensure test specimens are polished to reach a mirror-like surface finish, that is free of any micro scratches and uneven surfaces. Each of the sample sections were mounted in polymer epoxy and polished to an adequate level for indentation testing. Afterwards, the measurement data is collected over a spatial grid rather than just a line. The grid pattern was used when conducting indentation testing over specified distances and intervals on the surface of each sample. This should provide sufficient information for mapping the material properties of the interruption area. The specified grid was a 0.8 mm x 1.75 mm area with 5 points in x-direction at $\Delta x = 0.2 \text{ mm}$, and 8 points in y-direction at $\Delta y = 0.25 \text{ mm}$ resulting in total 40. Whereas for WAAM sample 90 indentation points were made with a grid of 5 points in x-direction at $\Delta x = 0.05 \text{ mm}$, and 18 points in y-direction at $\Delta y = 1 \text{ mm}$. A schematic of the testing grids, their distances, and intervals for each tiny sample are shown in Figure 13 & Figure 14.

Results are evaluated in the form of a mapping graph of the measurement points and their average values for each region (before interruption, amidst interruption, and after interruption). Finally, the indentation tests were done using a NHT2 indentation test machine (Anton Paar USA) shown in Figure 15 and a Vicker indenter. Table 4 presents the indentation testing parameters. From this analysis, the hardness can be determined as the ratio of the maximum load to the projected contact area [36]:

$$H_{IT} = \frac{F_{Max}}{A_p} \quad (1)$$

The Young's modulus of the material (E_{IT}) can be obtained from [37]:

$$M = \frac{E_{IT}}{1 - \nu_s^2} \quad (2)$$

here M denotes the indentation modulus and ν_s is the Poisson ratio of the material.

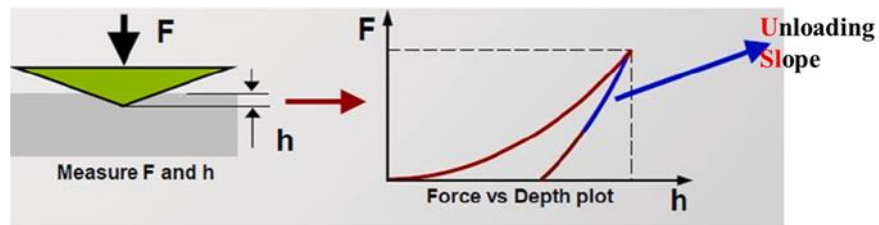


Figure 12. Measurement of load and penetration depth and related load-penetration curve

Table 4: Nano Indentation Parameters

Parameter	Measurement
	Example
Acquisition Rate	10 Hz
Loading Procedure	Linear
Max Load	75 mN
Loading/Unloading Rate	150 mN/min
Loading Pause Time	1.5 s
Approach Distance	3000 nm
Approach Speed	30000 nm/min
Retract Speed	2000 nm/min

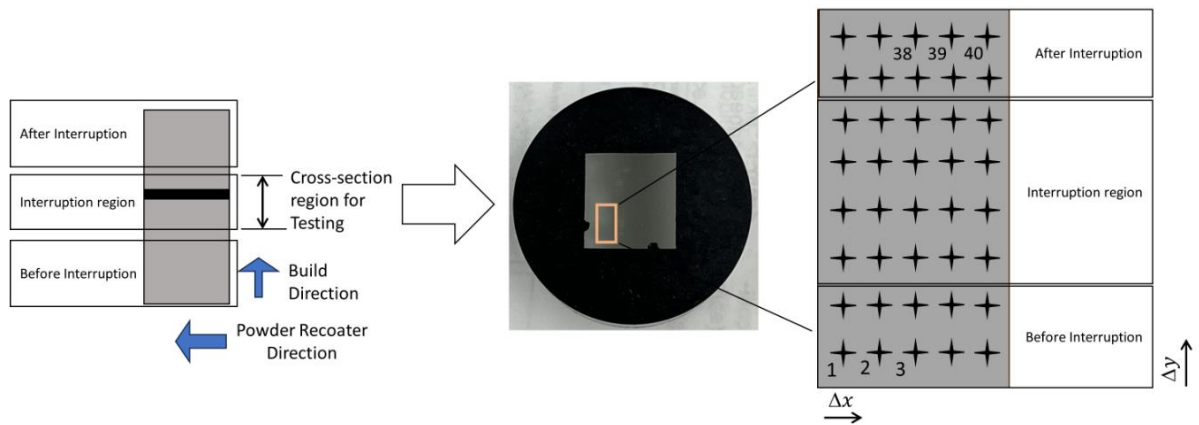


Figure 13. Matrix of the Indentation on the L-PBF samples

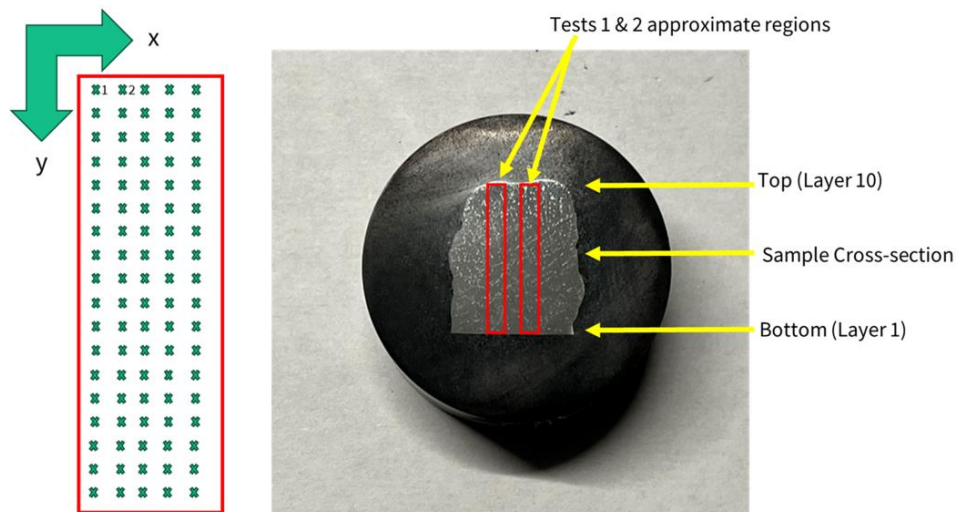


Figure 14. Indentation Matrix used for WAAM Samples

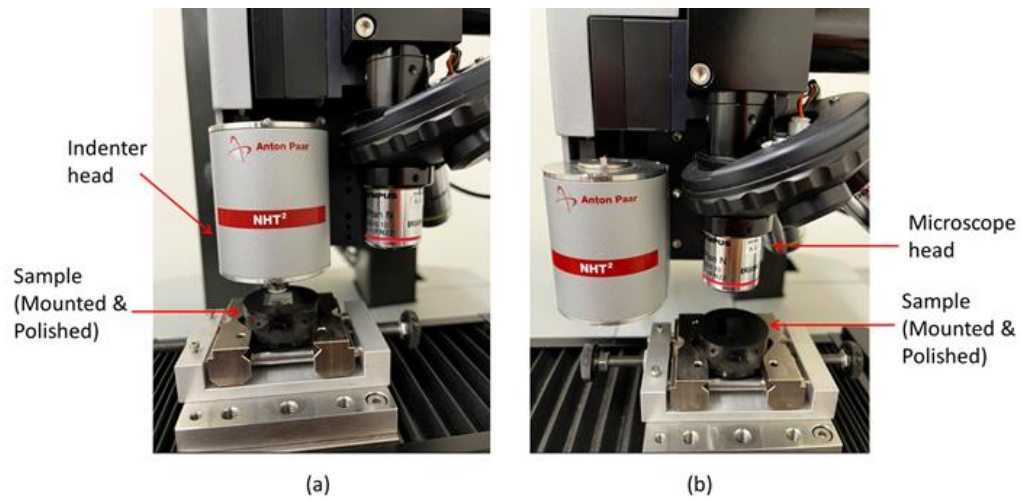


Figure 15. Sample Under the Nano Indenter- (a) Under the indenter head and (b) Under 20x microscope head

CHAPTER 4

DISCUSSION/RESULTS

4.1 Indentation test

4.1.1 L-PBF (Laser Powder Bed Fusion)

Figure 16 show the line graph of the hardness measurement results for as-built and heat-treated samples for before interruption, during interruption and after interruption, in comparison to within the groups Parameter A, D & E showed a significant change in their hardness values from each print whereas the change in between the prints from B & C was minimal in the as-built samples. In Parameter A,D & E print-1 showed higher hardness values compared to Print-2 & 3 with increase in interruption time the hardness of the samples decreased.

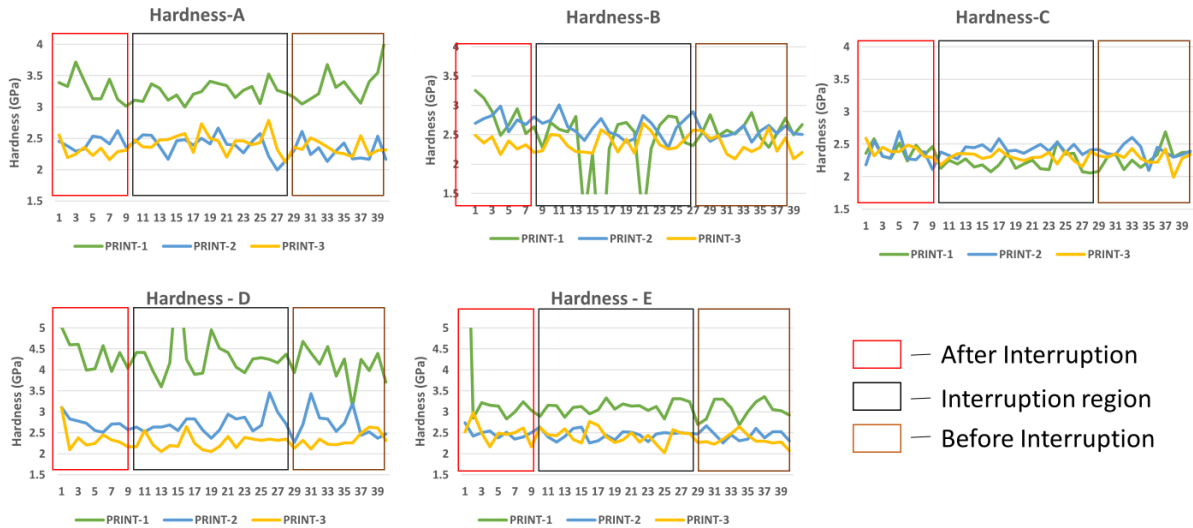


Figure 16. Mapping of Hardness values of as-built samples

Figure 17 shows the hardness results of heat-treated samples process interruptions have a noticeable impact on the hardness of the materials, affecting the consistency and potentially the quality of the final product. Stability generally returns post-interruption, but variability remains higher than in the pre-interruption phase.

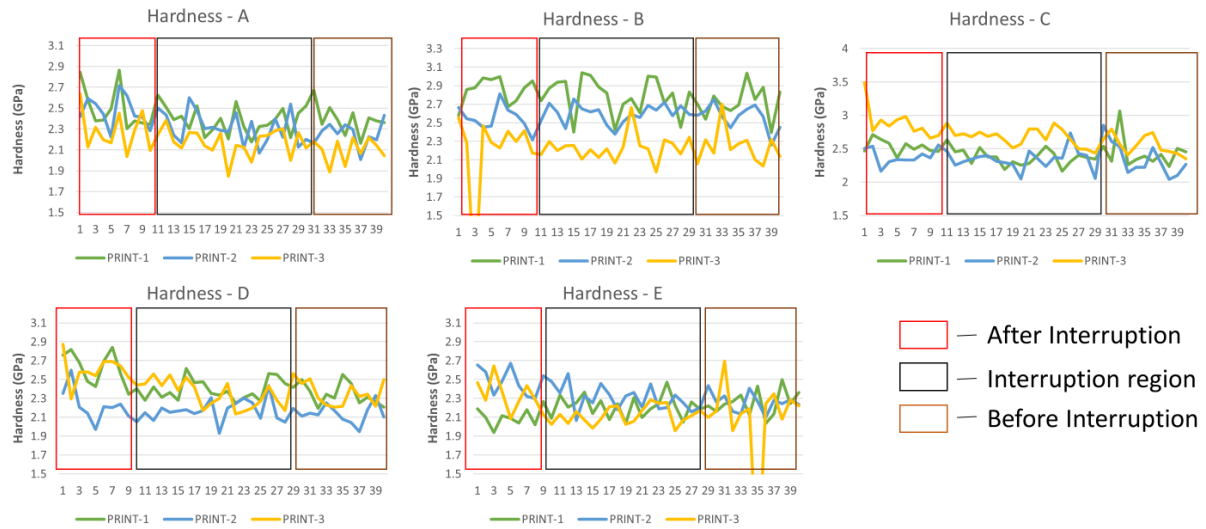


Figure 17. Mapping of Hardness values of Heat-treated samples

Figure 18 shows the comparison between the mean and standard deviation of three prints of as-built and heat-treated samples, the hardness values of heat treatment were lower with the parameters A, D & E but in case of parameter B & C the hardness of Heat-treated samples were slightly higher than as-built samples. Overall, when compared to as-built and heat-treated samples there was a huge variation with the increase in time from print-1 to print-3 in as-built samples, but whereas this variation was decreased or straightened within the heat-treated samples from print-1 to print-3.

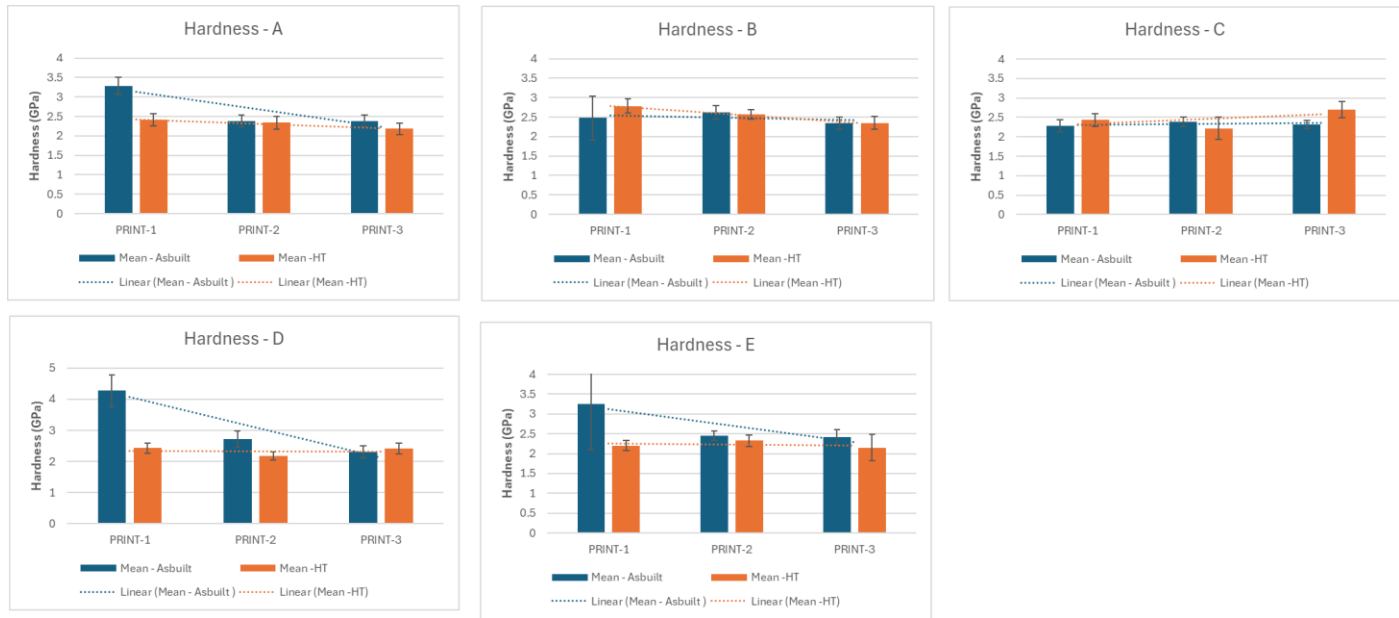


Figure 18. Mean & SD hardness comparison between As-built & Heat-treated L-PBF samples

The overall mean of Elasticity of the as-built samples decreased with the increase in the interruption time in all the parameters whereas for parameter B the elasticity increased with increase in interruption time. With comparison to as-built samples there was a huge variation in the elasticity whereas in heat treated samples the variation was decreased from print-1 to print-3 shown in Figure 19.

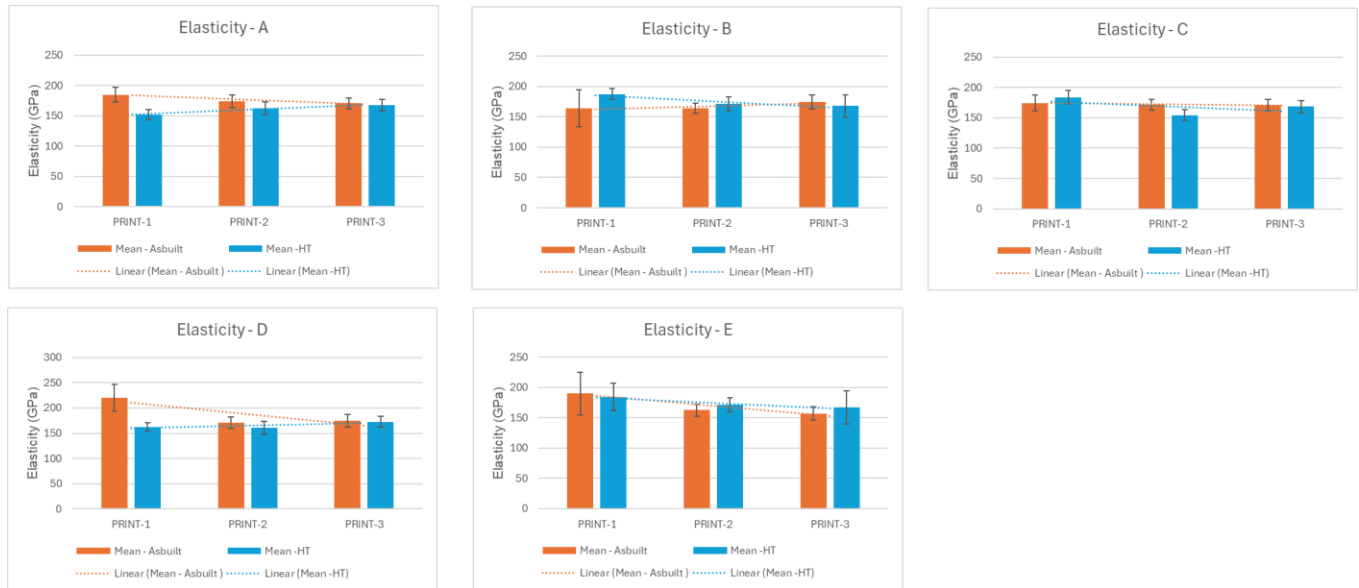


Figure 19. Mean & SD Elasticity comparison between As-built & Heat treated samples

4.1.2 WAAM Samples

Figure 20 shows the comparison between the hardness values of WAAM as-built and heat-treated samples demonstrates the impact of the comparison between the hardness values of WAAM as-built and heat-treated samples highlights the significant impact of heat treatment on the mechanical properties of WAAM-fabricated parts. This shows that heat treatment is a viable post-processing method to achieve more uniform hardness and potentially improve the structural integrity of an interrupted sample.

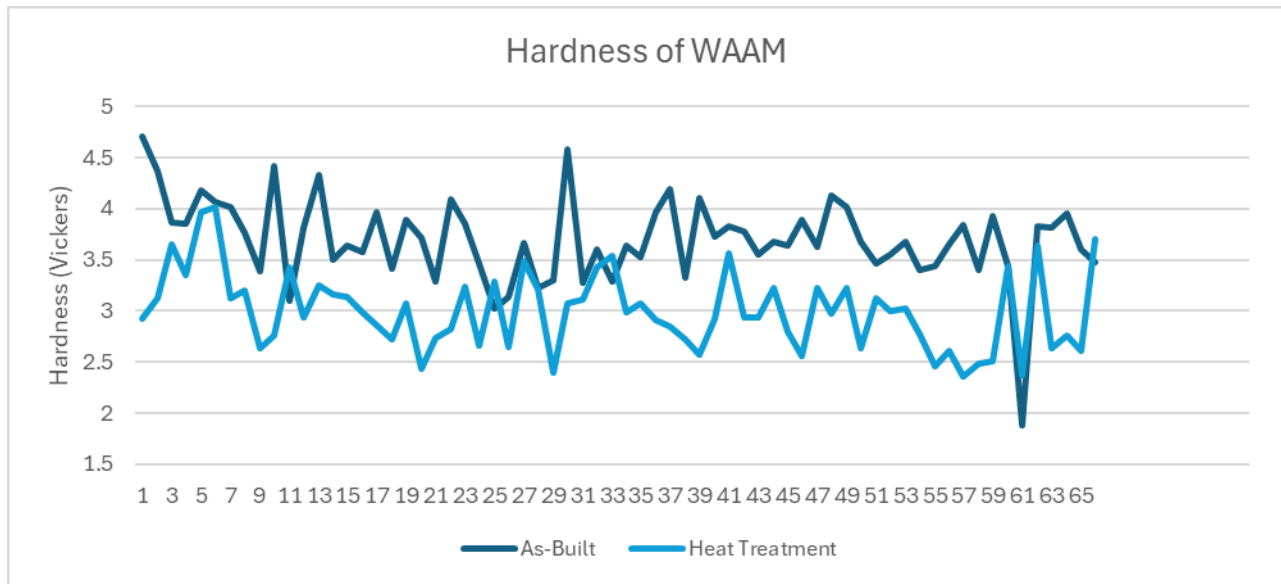


Figure 20. Comparison of Hardness values of all indentation on WAAM sample

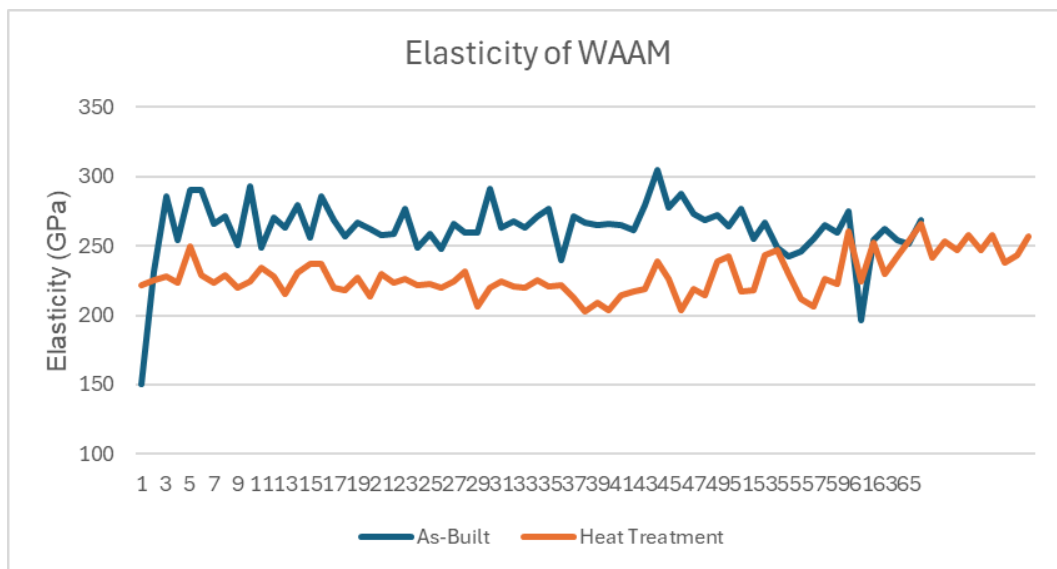


Figure 21. Comparison of Elasticity values of all indentation on WAAM sample

4.2 Statistical Analysis using ANOVA Test

Based on the data obtained from Nano Indentation test the data is being used to do Anova analysis of the samples, the data from interruption region is used to compare within and in-between the groups with a P value (critical value) of 0.05.

4.2.1 ANOVA analysis of L-PBF samples

Table 5 shows the Anova analysis of hardness values of As-Built samples for each print and each parameter, each parameter is compared with different prints. For e.g. Parameter A hardness values are compared with Print-1, Print-2 & Print-3 and other parameters B, C, D & E.

These results indicate that factors A, B, C, D, and E all have a statistically significant impact on the variability observed in the data, as their respective p-values are below the typical significance level of 0.05. This suggests that each factor (A, B, C, D, E) contributes significantly to explaining the variation in the dependent variable being studied. The critical F-value (F crit) of 3.158 is consistent across all factors, suggesting a common significance threshold used in the analysis.

Table 5: Hardness of As-Built of L-PBF samples

	Source of Variation	SS	df	MS	F	P-value	F crit
A	Between Groups	8.98	2	4.49	183.53	1.44653E-25	3.158
	Within Groups	1.39	57	0.02			
	Total	10.38	59				
B	Between Groups	0.97	2	0.4898	2.5707	0.085321	3.158
	Within Groups	10.86	57	0.1905			

	Total	11.84	59				
C	Between Groups	0.432	2	0.2164	25.4427	1.27E-08	3.158
	Within Groups	0.484	57	0.00850			
	Total	0.917	59				
D	Between Groups	46.842	2	23.4210	156.5665	6.99E-24	3.158
	Within Groups	8.526	57	0.1495			
	Total	55.368	59				
E	Between Groups	5.740	2	2.8701	116.4174	7.43E-21	3.158
	Within Groups	1.405	57	0.0246			
	Total	7.145	59				

Table 6 shows the Anova analysis of hardness values of HT samples for each print and each parameter, each parameter is compared within and in-between different prints and parameters.

This analysis shows that there is significant change between each parameter and within the parameter.

Table 6 : Hardness of HT Samples of L-PBF samples

	Source of Variation	SS	df	MS	F	P-value	F crit
A	Between Groups	0.462	2	0.2312	12.34	3.51E-05	3.158
	Within Groups	1.067	57	0.0187			
	Total	1.529	59				
B	Between Groups	3.292	2	1.6461	73.24	1.77E-16	3.158
	Within Groups	1.281	57	0.0224			
	Total	4.573	59				
C	Between Groups	1.195	2	0.5977	27.53	4.28E-09	3.158
	Within Groups	1.237	57	0.0217			
	Total	2.432	59				
D	Between Groups	0.583	2	0.2916	19.74	3.05E-07	3.158

	Within Groups	0.841	57	0.0147			
	Total	1.425	59				
E	Between Groups	0.288	2	0.1440	12.36	3.47E-05	3.158
	Within Groups	0.664	57	0.0116			
	Total	0.952	59				

Table 7 shows the elasticity of As-Built Samples which factors significantly impact the outcome, Factors A, B, D, and E show significant differences between groups, as indicated by their P-values being less than the critical value of 0.05. In contrast, Factor C does not show a significant difference, with a P-value of 0.39348, which is higher than 0.05. The F-value represents the ratio of between-group variance to within-group variance, with higher F-values indicating greater between-group variance. For a factor to be considered significant, its F-value must exceed the critical value of 3.158.

Table 7: Elasticity of As-Built of L-PBF samples

	Source of Variation	SS	df	MS	F	P-value	F crit
A	Between Groups	1476.89	2	738.44	10.26367	0.000156	3.158
	Within Groups	4101	57	71.94			
	Total	5577.89	59				
B	Between Groups	5137.091	2	2568.54	4.744508	0.012418	3.158
	Within Groups	30858.22	57	541.37			
	Total	35995.31	59				
C	Between Groups	175.67	2	87.83	0.948157	0.39348	3.158
	Within Groups	5280.52	57	92.64			
	Total	5456.19	59				
D	Between Groups	22540	2	11270	32.00845	4.8E-10	3.158
	Within Groups	20069.39	57	352.09			

	Total	42609.39	59				
E	Between Groups	7281.81	2	3640.90	32.83097	3.27E-10	3.158
	Within Groups	6321.22	57	110.89			
	Total	13603.04	59				

Table 8 represents the elasticity of HT samples fabricated using L-PBF samples, All five factors (A, B, C, D, and E) show significant differences between groups, with P-values below the critical value of 0.05. The F-values for all factors exceed the critical F-value of 3.158, reinforcing the significance of these results. Among the factors, Factor C has the most substantial impact, indicated by the highest F-value of 36.58. Factors A, B, and E also demonstrate strong impacts with F-values ranging from 10 to 12, while Factor D has a moderate impact with an F-value of 5.51.

Table 8: Elasticity of HT Samples of L-PBF samples

	Source of Variation	SS	df	MS	F	P-value	F crit
A	Between Groups	2275.19	2	1137.59	11.35	7.06E-05	3.158
	Within Groups	5710.03	57	100.17			
	Total	7985.22	59				
B	Between Groups	3262.24	2	1631.12	11.47	6.47E-05	3.158
	Within Groups	8098.81	57	142.08			
	Total	11361.06	59				
C	Between Groups	6211.44	2	3105.72	36.58	6.02E-11	3.158
	Within Groups	4839.25	57	84.89			
	Total	11050.7	59				
D	Between Groups	1193.03	2	596.51	5.51	0.006468	3.158
	Within Groups	6166.20	57	108.17			

	Total	7359.24	59				
E	Between Groups	3421.63	2	1710.81	10.027	0.000186	3.158
	Within Groups	9724.44	57	170.60			
	Total	13146.0	59				

4.2.2 ANOVA Analysis of WAAM Samples

Table 9 shows the Hardness of As-Built and HT treated Samples, the analysis reveals a statistically significant difference between groups, as evidenced by a P-value of 3.77E-09, which is substantially lower than the critical threshold of 0.05. This significance is further supported by the F-value of 56.29, greatly exceeding the critical F-value of 4.08. Additionally, the sum of squares between groups (5.84) surpasses the sum of squares within groups (4.15), highlighting that the variation between groups is more pronounced than the variation within groups.

Table 9: Hardness of As-built VS HT of WAAM sample

<i>Source of Variation</i>	<i>SS</i>	<i>df</i>	<i>MS</i>	<i>F</i>	<i>P-value</i>	<i>F crit</i>
Between Groups	5.84	1	5.84	56.29	3.77E-09	4.08
Within Groups	4.15	40	0.10			
Total	10.0	41				

Table 10 shows the Elasticity of As-Built and HT treated Samples the results demonstrate a highly significant difference between the groups, as indicated by the extremely low P-value (1.63E-15), which is far below the critical threshold of 0.05. This significance is further supported by the F-value (158.88), which greatly exceeds the critical F-value of 4.08. Additionally, the sum of squares between groups (25493.09) is substantially larger than the sum within groups (6417.80), indicating that the majority of the total variation (31910.89) is explained by the differences between groups.

Table 10 : Elasticity of As-built VS HT of WAAM sample

<i>Source of Variation</i>	<i>SS</i>	<i>df</i>	<i>MS</i>	<i>F</i>	<i>P-value</i>	<i>F crit</i>
Between Groups	25493.09	1	25493.09	158.88	1.63E-15	4.08
Within Groups	6417.80	40	160.44			
Total	31910.89	41				

4.3 Microscopic Images

The purpose of examining these microstructures is to understand the material's properties, its composition, how it was processed, and how it might perform under different conditions. This information is crucial in various fields such as materials science, metallurgy, geology, and biology, where understanding the internal structure of materials is essential for research, quality control, and development of new materials. The Images were taken using the microscope on Anton Par right after the testing is done, Figure 22 Shows the porosity line which is visible has been densified during the heat treatment process. This image was taken after the indentation is done and without any etchant solution

The interruption area is expected to be to be around 1-3 layers with a layer thickness of 0.03 mm, at the interruption region along with change in the grain size.

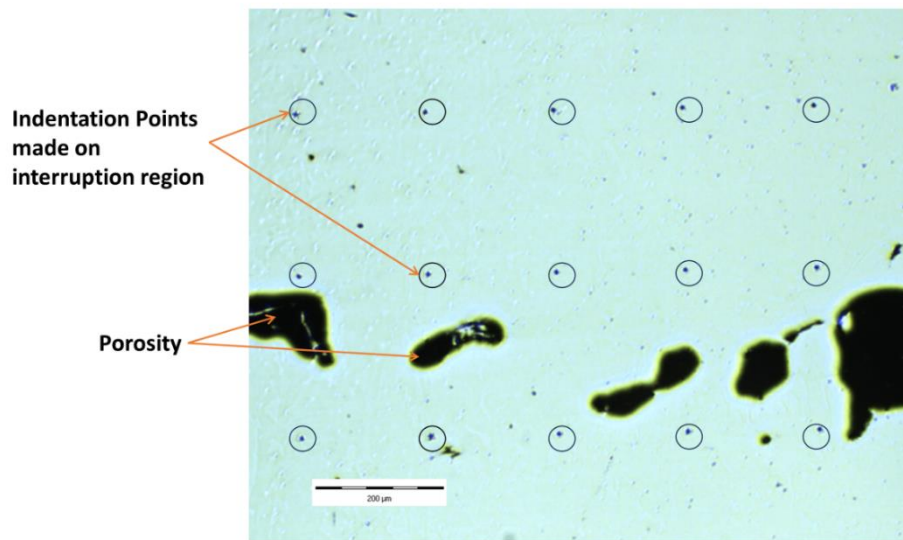


Figure 22. Indentation points with a porosity line on Print-3 for parameter E with 5x magnification (As-Built)

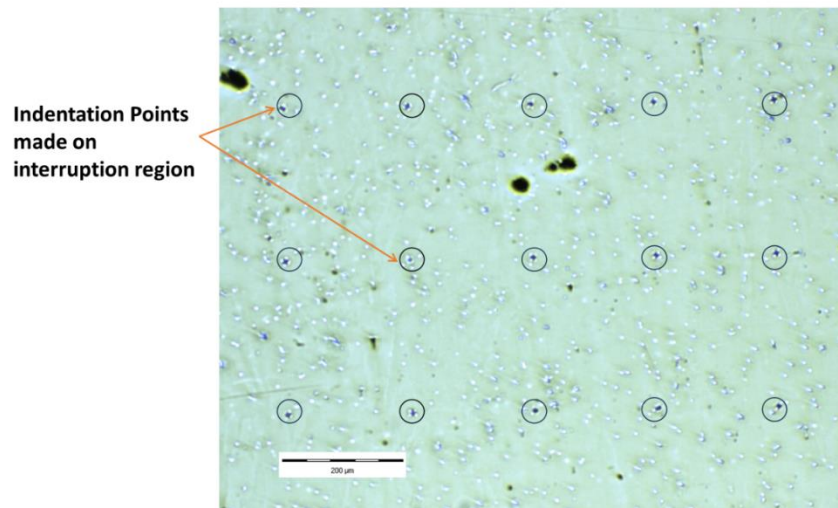


Figure 23. Indentation points without porosity line on Print-3 for parameter E with 5x magnification (Heat Treated)

Once the testing was finished, the samples were repolished and Etched using Marble's Reagent to examine how the parameters such as laser power and scan speed affect porosity formation with addition to the interruption period on As-Built and Heat treated samples. Etching is a process where a chemical solution is used to selectively remove material from the surface of a sample. This reveals the underlying microstructural features such as grain boundaries, phases, inclusions, and other details that may not be visible on the surface in their natural state. The images were taken using an optical microscope (Olympus Microscope). As mentioned earlier, these changes can impact the internal structure of the sample, influencing the overall quality of the part. This can lead to premature failure or inadequate mechanical properties. Figure 24 shows the microstructure of parameter B from Print-2 shows process interruption region, whereas on the other hand the grain structures around the interruption region seemed fairly uniform.



Figure 24. Print-2 of Parameter B under 20x magnification

Figure 25 shows the microstructure of parameter B from Print-3 shows process interruption region, whereas on the other hand the grain structures around the interruption region seemed un-uniform. But when compared to the Print-2 which has 2 hour interruption time, in print-3 the line is more uniform and is more clearly visible.

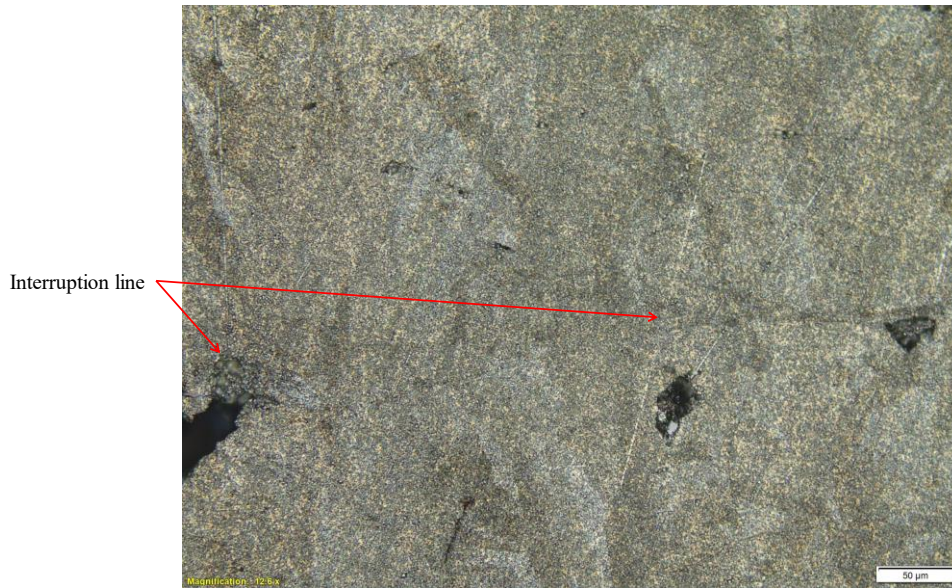


Figure 25. Print-3 of Parameter B under 20x magnification

4.4 Future Work

Throughout the experimentation many new problems were identified which open the scope for further study of this research when samples were printed, we had additional interruption region created on Print-1 or Built-1 on the last layers of the samples which can be investigated as they have a interruption period of 72 hours, samples can tested using different materials such as Titanium (Ti6AL4V), Aluminum and Inconel 718. The more number of interruption region at variable layers of a sample can be used to give us a better understanding of the impact on the

mechanical properties. The samples can be used for more material testing including NDT techniques (such as ultrasonic, CT) and SEM.

CHAPTER 5

CONCLUSION

The Impact of AM process interruption on mechanical properties of metal AM parts is experimentally evaluated. It is observed that there is a significant variation in the mechanical properties such as hardness and elasticity of the samples as the interruption time increases. This variation is more significant in hardness values compared to elasticity indicating a larger influence on the surface properties of the material rather than its bulk property (elasticity). However, utilizing post-processing methods such as heat treatment, the variation in material properties caused by process interruption is being more uniformed and the variation gap within the print is reduced.

The mechanical properties of the samples from Print-1 to Print-3 showed a decrease in hardness values. For the as-built parameter A (Optimum parameter), there was a 30% decrease in hardness from Print-1 to Print-2 and a 28% decrease from Print-1 to Print-3. However, when the samples were heat-treated, the differences in hardness values declined to 3% and 10%, respectively.

Out of all the 10 parameters (A, AH, B, BH, & EH) DH (with Laser power 225W and Scan Speed of 800mm/s) showed there was 65% of decrease in its hardness value and 22% decrease in its elasticity value, whereas DH on the other hand showed minimal changes in both hardness and elasticity with 2% and 5% from Print-1 to Print-3.

With the increase in scan speed (parameter E) had a inclination 21% in its hardness value and 14% in its elasticity value.

Within the Parameters, Parameter B (with lower Laser power) showed the minimal change in its hardness and

For further investigation can be done with comparing the results with samples without interruption and to also study how the cause of interruption affects the microstructure and grain orientation.

REFERENCES

- [1] W. M. Tucho, V. H. Lysne, H. Austbø, A. Sjolyst-Kvernland, and V. Hansen, “Investigation of effects of process parameters on microstructure and hardness of SLM manufactured SS316L,” *J Alloys Compd*, vol. 740, pp. 910–925, Apr. 2018, doi: 10.1016/j.jallcom.2018.01.098.
- [2] K. Chadha, Y. Tian, J. G. Spray, and C. Aranas, “Effect of annealing heat treatment on the microstructural evolution and mechanical properties of hot isostatic pressed 316L stainless steel fabricated by laser powder bed fusion,” *Metals (Basel)*, vol. 10, no. 6, pp. 1–18, Jun. 2020, doi: 10.3390/met10060753.
- [3] E. Liverani, S. Toschi, L. Ceschini, and A. Fortunato, “Effect of selective laser melting (SLM) process parameters on microstructure and mechanical properties of 316L austenitic stainless steel,” *J Mater Process Technol*, vol. 249, pp. 255–263, Nov. 2017, doi: 10.1016/j.jmatprotec.2017.05.042.
- [4] A. Kudzal *et al.*, “Effect of scan pattern on the microstructure and mechanical properties of Powder Bed Fusion additive manufactured 17-4 stainless steel,” *Mater Des*, vol. 133, pp. 205–215, Nov. 2017, doi: 10.1016/j.matdes.2017.07.047.
- [5] R. Li, Y. Shi, Z. Wang, L. Wang, J. Liu, and W. Jiang, “Densification behavior of gas and water atomized 316L stainless steel powder during selective laser melting,” *Appl Surf Sci*, vol. 256, no. 13, pp. 4350–4356, Apr. 2010, doi: 10.1016/j.apsusc.2010.02.030.
- [6] G. Wang, Q. Liu, H. Rao, H. Liu, and C. Qiu, “Influence of porosity and microstructure on mechanical and corrosion properties of a selectively laser melted

- stainless steel,” *J Alloys Compd*, vol. 831, Aug. 2020, doi: 10.1016/j.jallcom.2020.154815.
- [7] W. E. King *et al.*, “Observation of keyhole-mode laser melting in laser powder-bed fusion additive manufacturing,” *J Mater Process Technol*, vol. 214, no. 12, pp. 2915–2925, 2014, doi: 10.1016/j.jmatprotec.2014.06.005.
- [8] V. B. Vukkum and R. K. Gupta, “Review on corrosion performance of laser powder-bed fusion printed 316L stainless steel: Effect of processing parameters, manufacturing defects, post-processing, feedstock, and microstructure,” *Materials and Design*, vol. 221. Elsevier Ltd, Sep. 01, 2022. doi: 10.1016/j.matdes.2022.110874.
- [9] Y. S. Lee and W. Zhang, “Mesoscopic Simulation of Heat Transfer and Fluid Flow in Laser Powder Bed Additive Manufacturing.”
- [10] M. Mahtabi *et al.*, “Effects of Process Interruption During Laser Powder Bed Fusion on Microstructural and Mechanical Properties of Fabricated Parts.”
- [11] B. TITLE PAGE Ryan Mitchell Stokes and M. State, “Characterizing the effects of build interruptions on the microstructure and mechanical properties of powder bed fusion processed Al-Si-10Mg,” 2019.
- [12] M. Binder, C. Leong, C. Anstaett, G. Schlick, C. Seidel, and G. Reinhart, “Effects of process interruptions on the microstructure and tensile properties of AlSi10Mg parts manufactured by Laser-Based Powder Bed Fusion,” in *Procedia CIRP*, Elsevier B.V., 2020, pp. 182–187. doi: 10.1016/j.procir.2020.09.035.

- [13] V. Hammond, M. Schuch, and M. Bleckmann, "The influence of a process interruption on tensile properties of AlSi10Mg samples produced by selective laser melting," *Rapid Prototyp J*, vol. 25, no. 8, pp. 1442–1452, Sep. 2019, doi: 10.1108/RPJ-04-2018-0105.
- [14] F. Dababneh and H. Taheri, "Investigation of the influence of process interruption on mechanical properties of metal additive manufacturing parts," *CIRP J Manuf Sci Technol*, vol. 38, pp. 706–716, Aug. 2022, doi: 10.1016/j.cirpj.2022.06.008.
- [15] B. Gadagi and R. Lekurwale, "A review on advances in 3D metal printing," in *Materials Today: Proceedings*, Elsevier Ltd, 2020, pp. 277–283. doi: 10.1016/j.matpr.2020.10.436.
- [16] T. Duda and L. V. Raghavan, "3D metal printing technology: the need to re-invent design practice," *AI Soc*, vol. 33, no. 2, pp. 241–252, May 2018, doi: 10.1007/s00146-018-0809-9.
- [17] O. O. Salman *et al.*, "Selective laser melting of 316L stainless steel: Influence of TiB₂ addition on microstructure and mechanical properties," *Mater Today Commun*, vol. 21, Dec. 2019, doi: 10.1016/j.mtcomm.2019.100615.
- [18] J. Liu *et al.*, "Effect of scanning speed on the microstructure and mechanical behavior of 316L stainless steel fabricated by selective laser melting," *Mater Des*, vol. 186, Jan. 2020, doi: 10.1016/j.matdes.2019.108355.
- [19] E. Liverani, S. Toschi, L. Ceschini, and A. Fortunato, "Effect of selective laser melting (SLM) process parameters on microstructure and mechanical properties of

- 316L austenitic stainless steel,” *J Mater Process Technol*, vol. 249, pp. 255–263, Nov. 2017, doi: 10.1016/j.jmatprotec.2017.05.042.
- [20] T. R. Smith, J. D. Sugar, C. San Marchi, and J. M. Schoenung, “Strengthening mechanisms in directed energy deposited austenitic stainless steel,” *Acta Mater*, vol. 164, pp. 728–740, Feb. 2019, doi: 10.1016/j.actamat.2018.11.021.
- [21] Z. Zhang, B. Chu, L. Wang, and Z. Lu, “Comprehensive effects of placement orientation and scanning angle on mechanical properties and behavior of 316L stainless steel based on the selective laser melting process,” *J Alloys Compd*, vol. 791, pp. 166–175, Jun. 2019, doi: 10.1016/j.jallcom.2019.03.082.
- [22] A. Röttger, K. Geenen, M. Windmann, F. Binner, and W. Theisen, “Comparison of microstructure and mechanical properties of 316 L austenitic steel processed by selective laser melting with hot-isostatic pressed and cast material,” *Materials Science and Engineering: A*, vol. 678, pp. 365–376, Dec. 2016, doi: 10.1016/j.msea.2016.10.012.
- [23] C. R. Cunningham, J. M. Flynn, A. Shokrani, V. Dhokia, and S. T. Newman, “Invited review article: Strategies and processes for high quality wire arc additive manufacturing,” *Additive Manufacturing*, vol. 22. Elsevier B.V., pp. 672–686, Aug. 01, 2018. doi: 10.1016/j.addma.2018.06.020.
- [24] M. S. Hossain, A. Pliego, J. Lee, and H. Taheri, “Characterization of Wire-Arc Additively Manufactured (WAAM) of Titanium Alloy (Ti-6Al-4V) for Nanomechanical Properties,” in *Volume 2B: Advanced Manufacturing*, American Society of Mechanical Engineers, Nov. 2021. doi: 10.1115/IMECE2021-69673.

- [25] B. Wu *et al.*, “Effects of heat accumulation on the arc characteristics and metal transfer behavior in Wire Arc Additive Manufacturing of Ti6Al4V,” *J Mater Process Technol*, vol. 250, pp. 304–312, Dec. 2017, doi: 10.1016/j.jmatprotec.2017.07.037.
- [26] J. Richter, S. V. Sajadifar, and T. Niendorf, “On the influence of process interruptions during additive manufacturing on the fatigue resistance of AlSi12,” *Addit Manuf*, vol. 47, Nov. 2021, doi: 10.1016/j.addma.2021.102346.
- [27] C. A. Terrazas-Najera *et al.*, “Effects of process interruptions on microstructure and mechanical properties of three face centered cubic alloys processed by laser powder bed fusion,” *J Manuf Process*, vol. 66, pp. 397–406, Jun. 2021, doi: 10.1016/j.jmapro.2021.04.013.
- [28] M. Dinovitzer, X. Chen, J. Laliberte, X. Huang, and H. Frei, “Effect of wire and arc additive manufacturing (WAAM) process parameters on bead geometry and microstructure,” *Addit Manuf*, vol. 26, pp. 138–146, Mar. 2019, doi: 10.1016/j.addma.2018.12.013.
- [29] M. Akbari and R. Kovacevic, “An investigation on mechanical and microstructural properties of 316LSi parts fabricated by a robotized laser/wire direct metal deposition system,” *Addit Manuf*, vol. 23, pp. 487–497, Oct. 2018, doi: 10.1016/j.addma.2018.08.031.
- [30] W. S. Shin *et al.*, “Heat treatment effect on the microstructure, mechanical properties, and wear behaviors of stainless steel 316L prepared via selective laser

- melting,” *Materials Science and Engineering: A*, vol. 806, Mar. 2021, doi: 10.1016/j.msea.2021.140805.
- [31] K. Saeidi, S. Alvi, F. Lofaj, V. I. Petkov, and F. Akhtar, “Advanced mechanical strength in post heat treated SLM 2507 at room and high temperature promoted by hard/ductile sigma precipitates,” *Metals (Basel)*, vol. 9, no. 2, 2019, doi: 10.3390/met9020199.
- [32] M. S. I. N. Kamariah, W. S. W. Harun, N. Z. Khalil, F. Ahmad, M. H. Ismail, and S. Sharif, “Effect of heat treatment on mechanical properties and microstructure of selective laser melting 316L stainless steel,” in *IOP Conference Series: Materials Science and Engineering*, Institute of Physics Publishing, Nov. 2017. doi: 10.1088/1757-899X/257/1/012021.
- [33] O. O. Salman, C. Gammer, A. K. Chaubey, J. Eckert, and S. Scudino, “Effect of heat treatment on microstructure and mechanical properties of 316L steel synthesized by selective laser melting,” *Materials Science and Engineering: A*, vol. 748, pp. 205–212, Mar. 2019, doi: 10.1016/j.msea.2019.01.110.
- [34] R. F. Bishop, R. Hill, and N. F. Mott, “The theory of indentation and hardness tests,” *Proceedings of the Physical Society*, vol. 57, no. 3, pp. 147–159, May 1945, doi: 10.1088/0959-5309/57/3/301.
- [35] F. Yan, W. Xiong, and E. J. Faierson, “Grain structure control of additively manufactured metallic materials,” *Materials*, vol. 10, no. 11, p. 1260, Nov. 2017, doi: 10.3390/ma10111260.

- [36] *Industrializing Additive Manufacturing - Proceedings of Additive Manufacturing in Products and Applications - AMPA2017*. Cham: Springer International Publishing, 2018. doi: 10.1007/978-3-319-66866-6.
- [37] P. C. Collins, D. A. Brice, P. Samimi, I. Ghamarian, and H. L. Fraser, “Microstructural Control of Additively Manufactured Metallic Materials,” *Annual Review of Materials Research*, vol. 46. Annual Reviews Inc., pp. 63–91, Jul. 01, 2016. doi: 10.1146/annurev-matsci-070115-031816.